iScience

CellPress
OPEN ACCESS

Article

Direct visualization of general anesthetic propofol on neurons by stimulated Raman scattering microscopy

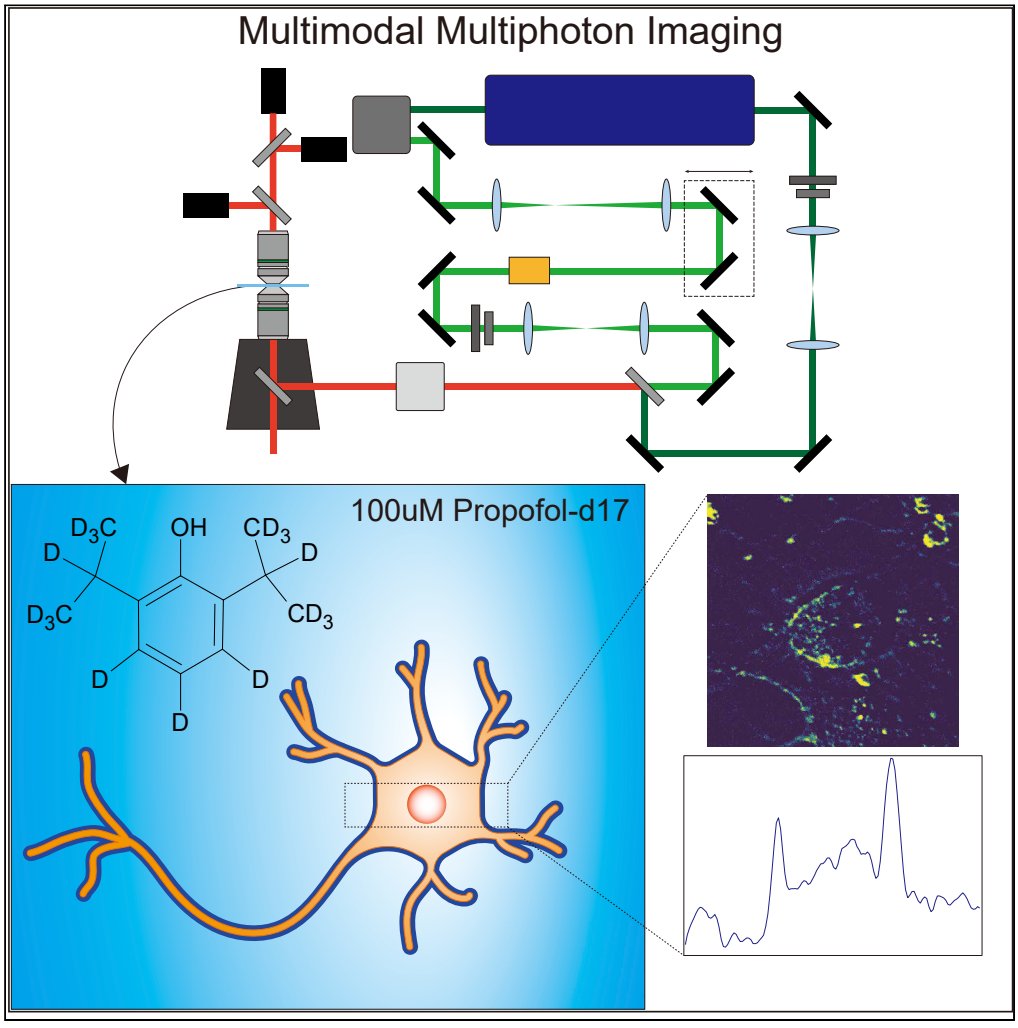

Robert Oda,
Jingwen Shou,
Wenying Zhong,
Yasuyuki Ozeki,
Masato Yasui,
Mutsuo Nuriya

rwoda@keio.jp (R.O.)
mnuriya@keio.jp (M.N.)

Highlights

Multi-modal SRS developed for real-time biological imaging of small molecule substances

Propofol primarily concentrates at the cell membrane of neurons

Anesthesia dynamics can be monitored in real-time with SRS

Oda et al., iScience 25, 103936
March 18, 2022
https://doi.org/10.1016/j.isci.2022.103936

iScience

CellPress
OPEN ACCESS

Article

Direct visualization of general anesthetic propofol on neurons by stimulated Raman scattering microscopy

Robert Oda,[1,2,5,*] Jingwen Shou,[2] Wenying Zhong,[1] Yasuyuki Ozeki,[2] Masato Yasui,[1] and Mutsuo Nuriya[1,3,4,*]

SUMMARY

The consensus for the precise mechanism of action of general anesthetics is through allosteric interactions with GABA receptors in neurons. However, it has been speculated that these anesthetics may also interact with the plasma membrane on some level. Owing to the small size of anesthetics, direct visualization of these interactions is difficult to achieve. We demonstrate the ability to directly visualize a deuterated analog of propofol in living cells using stimulated Raman scattering (SRS) microscopy. Our findings support the theory that propofol is highly concentrated and interacts primarily through non-specific binding to the plasma membrane of neurons. Additionally, we show that SRS microscopy can be used to monitor the dynamics of propofol binding using real-time, live-cell imaging. The strategy used to visualize propofol can be applied to other small molecule drugs that have been previously invisible to traditional imaging techniques

INTRODUCTION

In the operating room, propofol (2,6-diisopropylphenol) is routinely used as a means of general anesthetic. Propofol is intravenously administered and is a popular choice among surgeons for inducing a sedative effect on patients and is also used for maintenance of sedation in other areas such as intensive care unit (Feng et al., 2017). While it is widely used and routinely administered, the exact mechanism of action and interactions in the body are not clearly understood. Because propofol does exhibit some level of toxicity to neurons (Kahraman et al., 2008), it is important to understand the underlying mechanisms of propofol's action. While evidence suggests that propofol potentiates $GABA_A$ receptors (Hales and Lambert, 1991; Hemmings et al., 2005; Yip et al., 2013), its effect on other ion channels is also suggested (Lugli et al., 2009; Urban et al., 2006; Yang et al., 2015, 2018). In addition to protein-specific interactions, it has also been hypothesized that anesthetics interact with the plasma membrane of cells to induce hypnosis (Pavel et al., 2020; Tsuchiya and Mizogami, 2013). However, at the cellular level, propofol has never been directly imaged as it interacts with cells. Owing to this lack of direct evidence of these interactions, pharmacological understandings of propofol's activity at the molecular/cellular levels remains elusive, which can hinder the development of new anesthetics.

This lack of direct visualization of propofol is due to its small size. In traditional fluorescence microscopy, bulky fluorophores are used to image various substances within cells and tissue. In the case of these small molecules (e.g., propofol has a molecular weight of 178.3, fluorophores can far exceed the size of the molecule in question (e.g., Alexa 488 has a molecular weight of 643.4) and will inevitably interfere with the activity of the molecule itself when conjugated. Therefore, to characterize the dynamics of propofol and other small-sized drugs, new approaches other than conventional fluorescence tagging/imaging is needed.

Recently, many studies have been conducted on stimulated Raman scattering (SRS) microscopy as a potential tool to analyze and probe the dynamics of biological substances on cells and tissue (Cheng and Xie, 2015; Hill and Fu, 2019; Hu et al., 2019; Ozeki, 2020; Zhang and Cheng, 2018). The Raman scattering effect is the inelastic collision of light particles (photons) with molecular bonds (Raman and Krishnan, 1928). By exploiting the shifts in photon energy, it is possible to obtain spectral "fingerprints" of a biological sample's molecular structure. While spontaneous Raman scattering has been applied to detection of biological substances such as drugs previously (Huser and Chan, 2015; Paidi et al., 2016), the utility of spontaneous Raman is limited by its long acquisition time which hinders its ability to image live cells and to characterize

[1]Department of Pharmacology, School of Medicine, Keio University, 35 Shinanomachi, Shinjuku, Tokyo 160-8582, Japan

[2]Department of Electrical Engineering and Information Systems, Graduate School of Engineering, 7-3-1 Hongo, Bunkyo, Tokyo 113-8656, Japan

[3]Graduate School of Environment and Information Sciences, Yokohama National University, 79-1 Tokiwadai, Hodogaya, Yokohama, Kanagawa 240-8501, Japan

[4]Precursory Research for Embryonic Science and Technology (PRESTO), Japan Science and Technology Agency (JST), 4-1-8 Honcho, Kawaguchi, Saitama 332-0012, Japan

[5]Lead contact

*Correspondence: rwoda@keio.jp (R.O.), mnuriya@keio.jp (M.N.)

https://doi.org/10.1016/j.isci.2022.103936

the dynamics of drugs at high temporal resolution. To accelerate the imaging speed, SRS is comprised of a two-laser system: a pump beam and a Stokes beam. By tuning the frequency difference of the two light fields to match the molecular vibration of target molecules, the contrast at different wavenumbers can be obtained. With SRS, the rapid identification of the Raman signals becomes possible, which is more conducive for live-cell imaging (Ozeki et al., 2012; Saar et al., 2010).

SRS microscopy has great advantage over fluorescence microscopy in that it can readily identify Raman-tags of small molecular weight; this allows researchers to probe small molecules that would be previously invisible to traditional tools. One application of SRS is that it can visualize deuterated substances (Fu et al., 2014; Hu et al., 2014; Saar et al., 2011; Wei et al., 2013; Zhang et al., 2011, 2019). Deuterium substitution is minimally invasive and can be detected at high sensitivity with distinct Raman scattering signals in the silent region, making it an ideal Raman-tag. Previously, spontaneous Raman spectroscopy has been used to detect anesthetics in blood and solution (Nwaneshiudu et al., 2014; Wróbel et al., 2015). However, this is still indirect evidence of the interactions these anesthetics have on cells. SRS has never been used before to directly image anesthetic drugs in cells. Because propofol is a small substance that cannot be easily visualized with traditional methods, we propose SRS as a vital tool to understanding the dynamics of anesthesia on neurons. Here, we report the first direct images of a deuterated analog of propofol (propofol-d17) and its interactions on neurons using SRS and describe our system's capability to image and track the dynamics of propofol-d17 on living hippocampal neurons.

RESULTS

Propofol-d17 acts as a physiological Raman probe

Our SRS system (Figure 1A) allows for imaging of samples at specific Raman wavenumbers (Mizuguchi et al., 2021). By tuning the wavelength of the pump pulses from an optical parametric oscillator, we can select any desired Raman wavenumber for imaging. In the silent region of the Raman spectra (1800–2800 cm^{-1}), it is possible to image substances containing alkynes and deuterium due to their unique spectra and lack of competing signals originating from various molecules in biological samples. Propofol-d17 (Figure 1B) is an analog of normal propofol with every hydrogen replaced with deuterium atoms (Hese et al., 2020; Mannocchi et al., 2013). The Raman spectrum of propofol-d17 (Figure 1C) was first obtained using an SRS system with wide tunability in order to identify at which wavelength our system will image deuterated propofol (Ozeki et al., 2019; Shou et al., 2021). The spectrum shows many distinct peaks in the silent region of the Raman spectra that are unique to propofol-d17.

We first established that our system can image deuterated substances using glucose-d6 and palmitic acid-d31 in HeLa cells (Zhang et al., 2011, 2019) (Figures S1A and S1B). Because Raman scattering signals are specific, the signal of deuterated palmitic acid and glucose should disappear when imaged at a wavenumber that does not possess a Raman signal. In both palmitic acid and glucose, we observe that the signal disappears when imaged off-Raman peak. In addition, our imaging system is equipped with photomultiplier tubes to detect other non-linear optical processes including two-photon excited fluorescence, resulting in simultaneous multi-modal imaging. To test this multi-modal imaging capacity, we then imaged primary cultured hippocampal neurons with palmitic acid-d31 and imaged both on and off-Raman signal in combination with calcein-AM that fills up and labels the cytoplasm of the cells (Figure S2). Like HeLa cell imaging, we were able to get a strong SRS signal on peak which disappears when imaging the off-Raman signal. Furthermore, we could successfully obtain strong two-photon excited fluorescence signals of calcein-AM simultaneously with SRS, which is insensitive to the small wavelength differences between on and off-Raman peaks and reflects differences in the peak spectral width of SRS and two-photon excited fluorescence.

With the ability to image deuterated substances in neurons established, we then verified that deuterated propofol behaves in a similar manner to normal propofol (Helfenbein et al., 2002). Calcium imaging experiments using the calcium indicator Fluo4-AM show that after introduction of normal propofol, action potential-induced calcium spikes of primary cultured hippocampal neurons are silenced, as would be expected for general anesthetic. This is also seen after the introduction of propofol-d17 onto neurons (Figure 1D). Because propofol is dissolved in DMSO, the acute effects of DMSO were assessed as a negative control. Addition of the same amount of DMSO to the cell culture without any propofol or deuterated propofol did not inhibit the calcium signaling of neurons (Figure S3). These data demonstrate that propofol-d17 maintains the pharmacological activity, suggesting that propofol-d17 serves as an authentic Raman probe of propofol.

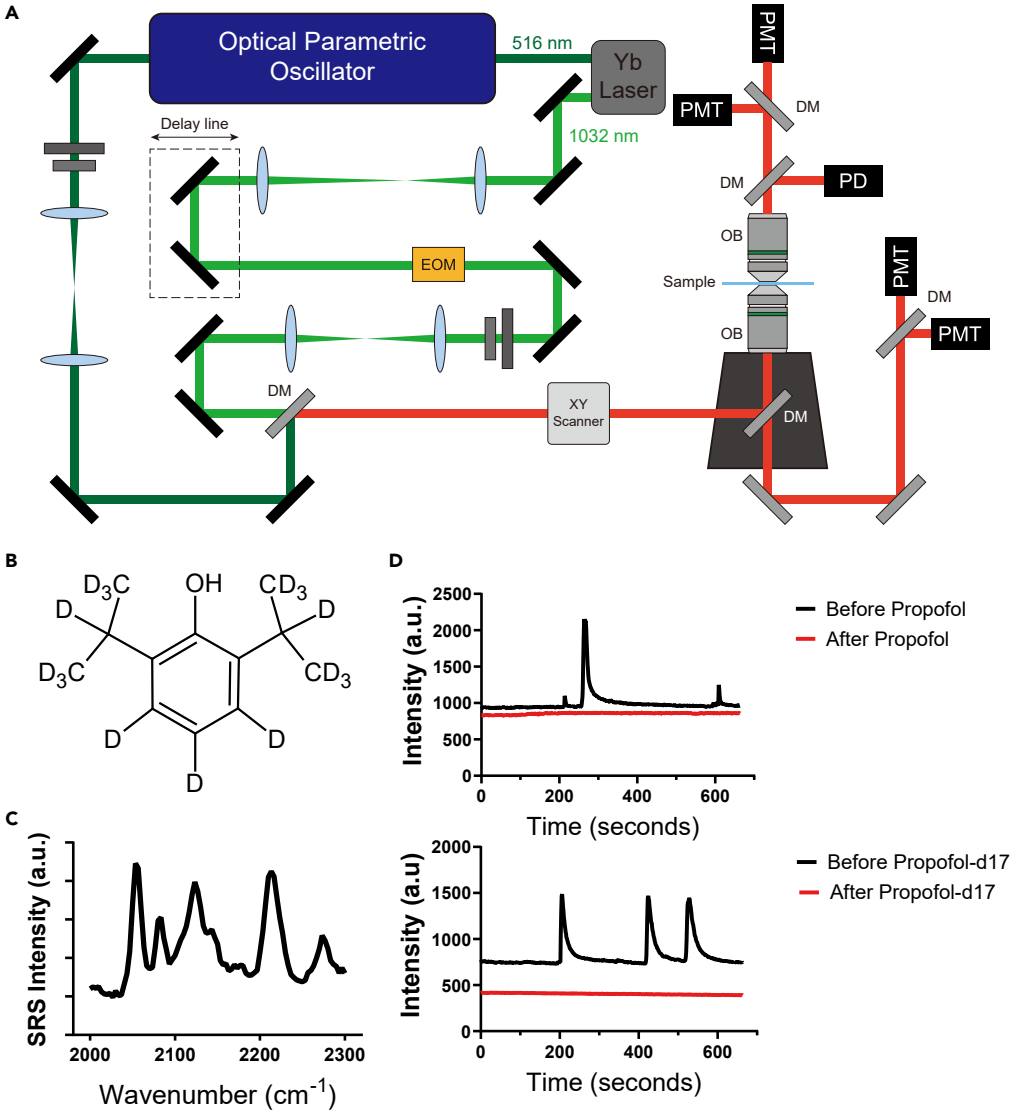

Figure 1. Characterization of propofol-d17 as a Raman probe for general anesthesia

(A) A detailed schematic of our SRS system is shown. Each PMT can be fitted with a bandpass filter for detection of different signals (e.g., two-photon excited fluorescence). A maximum of 4 unique signals are possible in combination with SRS.

(B) Chemical drawing of the structure of propofol-d17.

(C) Raman spectra of 100 mM propofol-d17 in DMSO. Spectra were obtained using a scanning SRS microscope.

(D) Pharmacological characterization of propofol and propofol-d17. Fluo4-AM-loaded primary culture neurons shows calcium spikes. After the introduction of propofol and propofol-d17, calcium signaling is silenced and no spikes are observed in the same amount of observation time. (DM, dichroic mirror; PMT, photomultiplier tube; PD, photodiode detector)

Propofol-d17 interacts primarily with the plasma membrane of neurons

After characterization of propofol, we then proceeded to image propofol-d17 directly in primary cultured hippocampal neurons. Propofol-d17 was applied directly to the extracellular solution of the cultured neurons and immediately imaged in the continuous presence of propofol-d17. Using the 2,055 cm^{-1} as the on Raman-peak, and 2,000 cm^{-1} as off-Raman, we obtained high-resolution images of propofol-d17 in living neurons (Figure 2). Interestingly, the signal appears to be high at the cellular membrane of the neuronal cell body and neurites (Figure 3), even though propofol-d17 still existed in the extracellular solution.

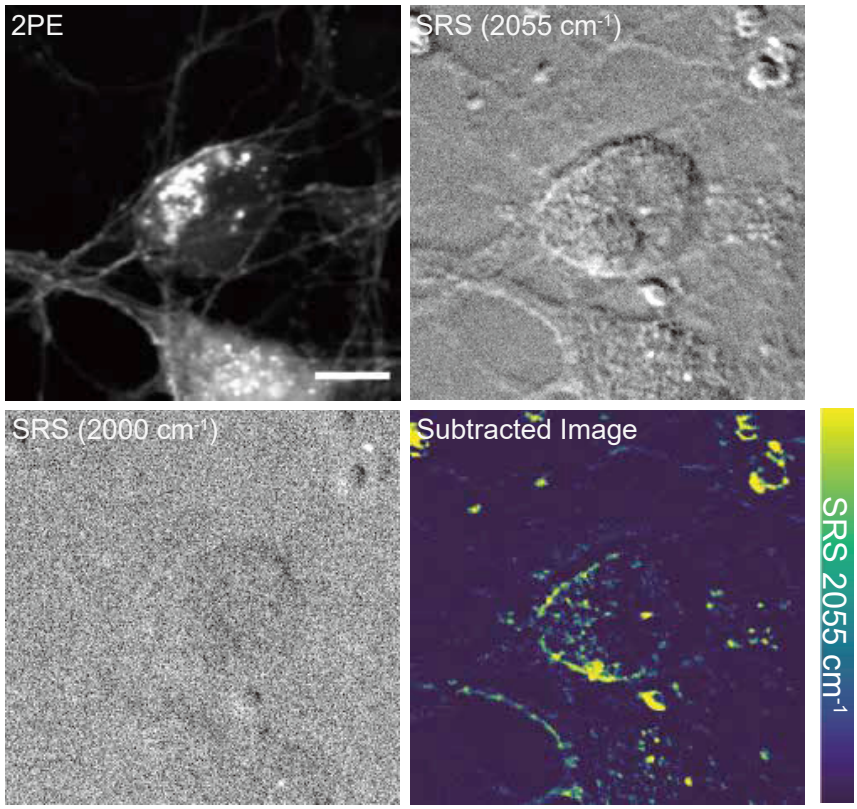

Figure 2. Direct imaging of propofol-d17 by SRS microscopy at 2055 cm^{-1} (on-Raman) and 2000 cm^{-1} (off-Raman)
Two-photon excited calcein-AM fluorescence imaging (2PE) taken simultaneously with SRS imaging serves as a guide to the distribution of propofol on the cell. The intensity is highest at the cell membrane of the cell body and is also visible on the membrane of the neurites (scale bar = 10 μm)

To confirm this observation, we measured the intensity of propofol signals across the cell membrane of the cell body and neurites. By projecting a box across the cellular membrane of neurites and cell bodies of the neuron, we measured the intensity profiles of the SRS signal with the reference of cellular positions from the intensity profiles of simultaneously obtained two-photon excited fluorescence signals of calcein-AM. This analysis revealed that the propofol SRS signal is indeed higher at cell membrane when compared to the outside and inside of the cell. As the projection crosses the cell membrane of the cell, our data suggest a higher concentration of propofol at the membranes when compared to the inside and outside of the cell body (Figures 3A and 3B). This method of quantifying concentration was applied to multiple imaged cells (n = 16); it was found that the average estimated concentration of propofol-d17 at the cell membrane was 130.1 ± 22.58 μM (mean ± SD), assuming the extracellular solution remains at 100 μM (Figure 3C) (see discussion for detail).

We then investigated the potential mechanisms of the specific localization of propofol at the plasma membrane. First, we investigated the localization of $GABA_A$ receptors on the neurons by immunocytochemistry. The obtained images showed that there was a non-uniform distribution of $GABA_A$ receptors at the plasma membrane of the neurons (Figure 4A), consistent with the idea of $GABA_A$ receptors' clustering at synaptic sites (Thomson and Jovanovic, 2010; Tretter et al., 2008). Propofol is widely considered to interact primarily with $GABA_A$ receptors (Krasowski et al., 1997; Yip et al., 2013), but our data show that the distribution of propofol-d17 and these receptors are not the same. This suggests that the primary force driving localization of propofol on the plasma membrane is its affinity to the plasma membrane itself and not its specific binding to $GABA_A$ receptors. We imaged propofol-d17 on HeLa cells to test this idea. It has been previously reported that propofol could disrupt the microstructure of the plasma membrane in cancerous cell lines (Zhang et al., 2016). Similarly, it was reported that propofol reduces the permeability of the plasma membrane of leukemia cells (Reitz et al., 1999), but this data were

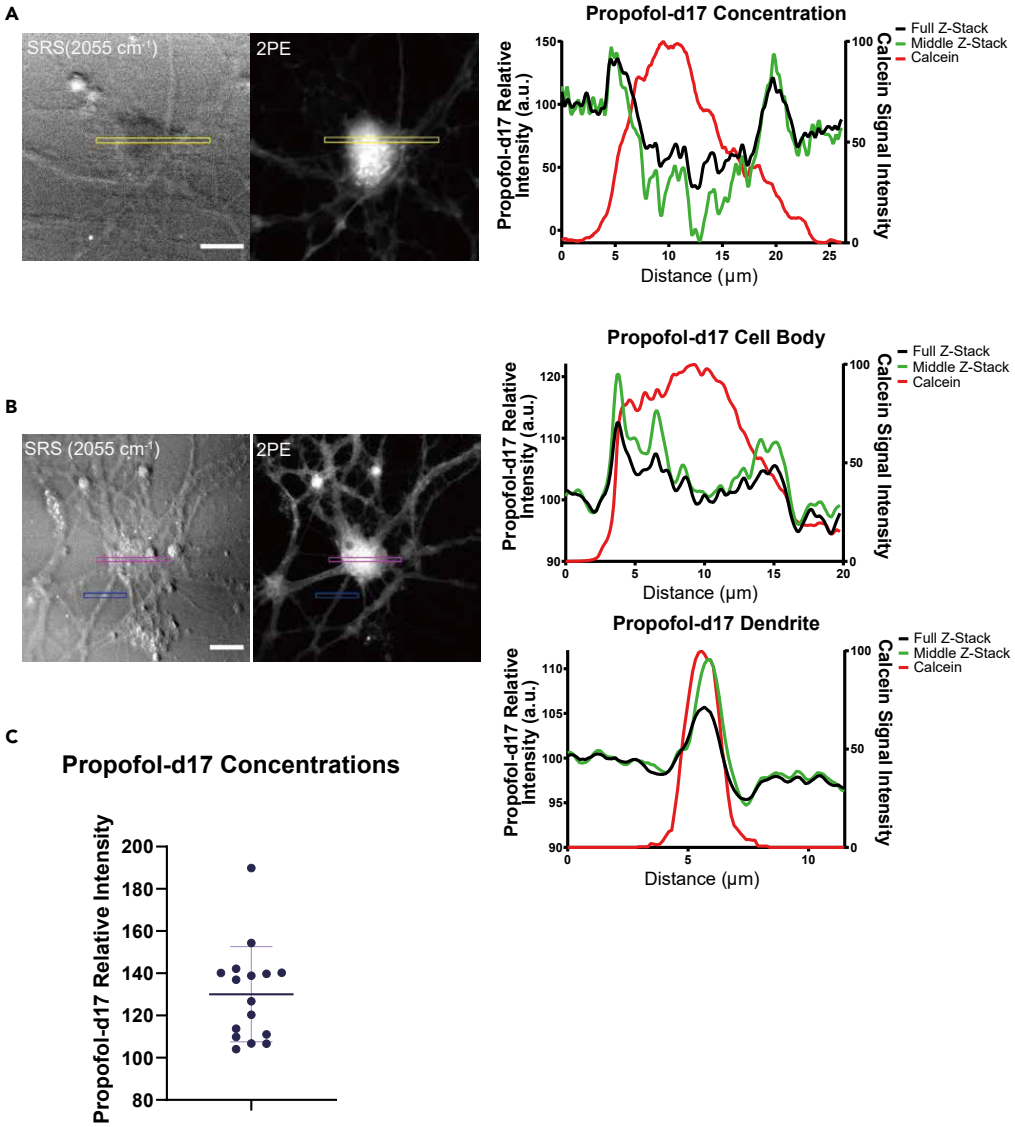

Figure 3. Propofol localizes at the cell membrane of neurons at both the cell body and at the dendrites

(A) Measurement of the intensity of SRS signal across the cellular membrane of the cell body of a neuron shows that there is an increase in signal at the cell membrane and there is lower signal inside and outside of the cell itself. Calcein-AM signal intensity was normalized and plotted to show the boundary of the cell. Increase in calcein-AM signal corresponds to the boundary of the cell body and matches the increase in SRS signal at the plasma membrane (scale bar = 10 μm).

(B) SRS of propofol-d17 also reveals localization of anesthesia at both cell body and dendrites. Measurements across the membrane of both cell body and dendrite show an increase in SRS signal across the cellular membranes and a decrease in signal when measured off target. Intensities are measured as a projection across an averaged section of each box using built-in ImageJ functions. Each image was first initially imaged as a full z stack averaged together (10 slices); an additional measurement was taken from and averaging of the middle 5 Z-stacks to create an image from the middle of the cell (scale bar = 10 μm).

(C) Measurements of the local intensity of SRS signal at the cell membrane of multiple neurons (n = 16) were used to calculate estimated concentration. The average estimated concentration of propofol-d17 at the cell membrane was 130.1 ± 22.58 μM (mean ± standard deviation)

collected through indirect methods such as electroporation and trypan blue. We successfully obtained direct imaging of HeLa cells and calculated the estimated concentration of propofol on the plasma membrane (Figure 4B). We confirmed the presence of propofol on the membrane of HeLa cells, and the estimated propofol concentration at the cell membrane of HeLa cells were like the concentrations found on

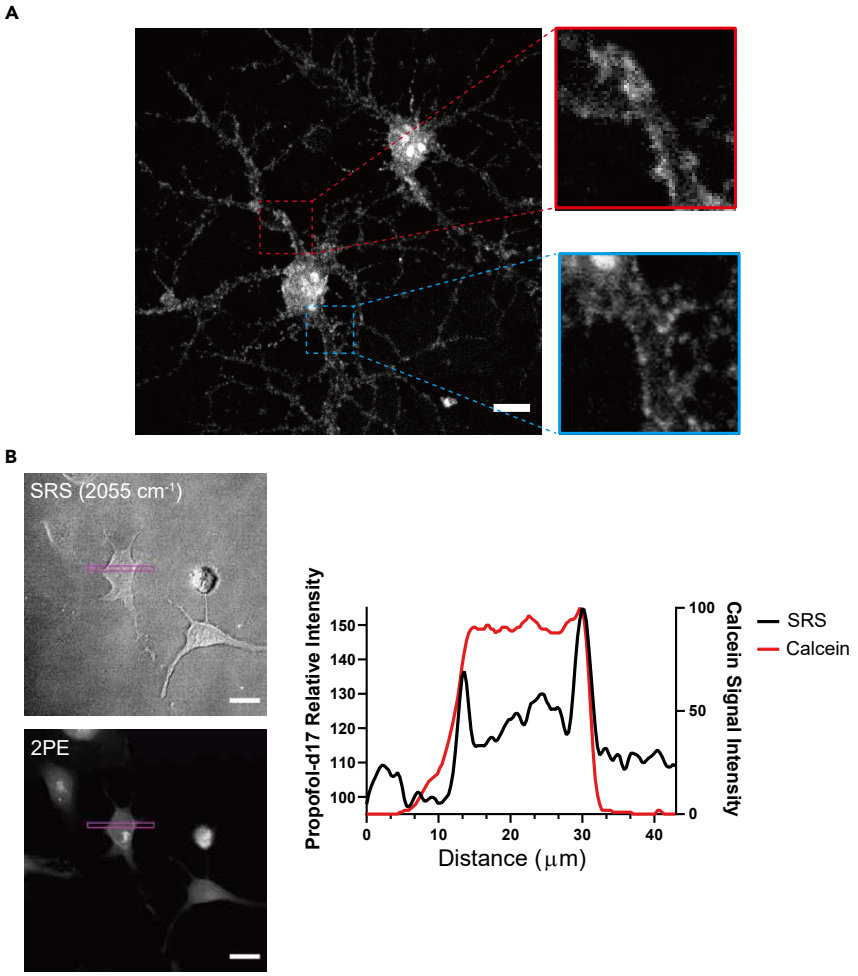

Figure 4. Propofol-d17 localizes primarily on the plasma membrane

(A) Immunofluorescent imaging of $GABA_A$ receptors on neurons. Along the neurites of the neurons, sharp signals indicate that a non-uniform distribution of receptors along the neurites on the cell membrane (scale bar = 20μm).

(B) Propofol measurements on the cell membrane of HeLa cells. The same, uniform distribution of propofol-d17 SRS signals was observed in the cell membrane of HeLa cells. Measurements of the estimated concentration of propofol-d17 show similar results to neuronal data (scale bar = 20μm)

the cell membrane of neurons, even though HeLa cells do not express $GABA_A$ receptors (Figure S4). This lends further evidence toward the idea that propofol's localization at the plasma membrane is mainly achieved by its affinity to the hydrophobic environment of the plasma membrane and not via its direct binding to the $GABA_A$ receptors. Based on our data, we propose that propofol first localizes to the plasma membrane rather nonspecifically, and then binds to and acts on the $GABA_A$ receptors and potential other targets through probabilistic collision and following binding during lateral diffusions inside the plasma membrane.

Propofol-d17 binding can be tracked by SRS microscopy

Finally, we carried out experiments to characterize the dynamics of propofol. The high sensitivity of our SRS imaging system allowed us to monitor dynamics of propofol on the same neurons (Figure 5A). Time-lapse images of propofol were captured using our SRS system by creating grouped averages of images over the course of continuous propofol perfusion (Figure 5B). Initially, cells were imaged with propofol-d17 and continued to be imaged with a continuous perfusion of non-deuterated propofol at the same concentration. Analysis of the intensity of propofol signals of the cells showed a decrease in SRS intensity which suggests the quick replacement of propofol-d17 by new incoming propofol (Figure 5C). Additionally, this decrease in SRS signal of propofol-d17 can be modeled by an exponential decay curve (Figure 5D). These

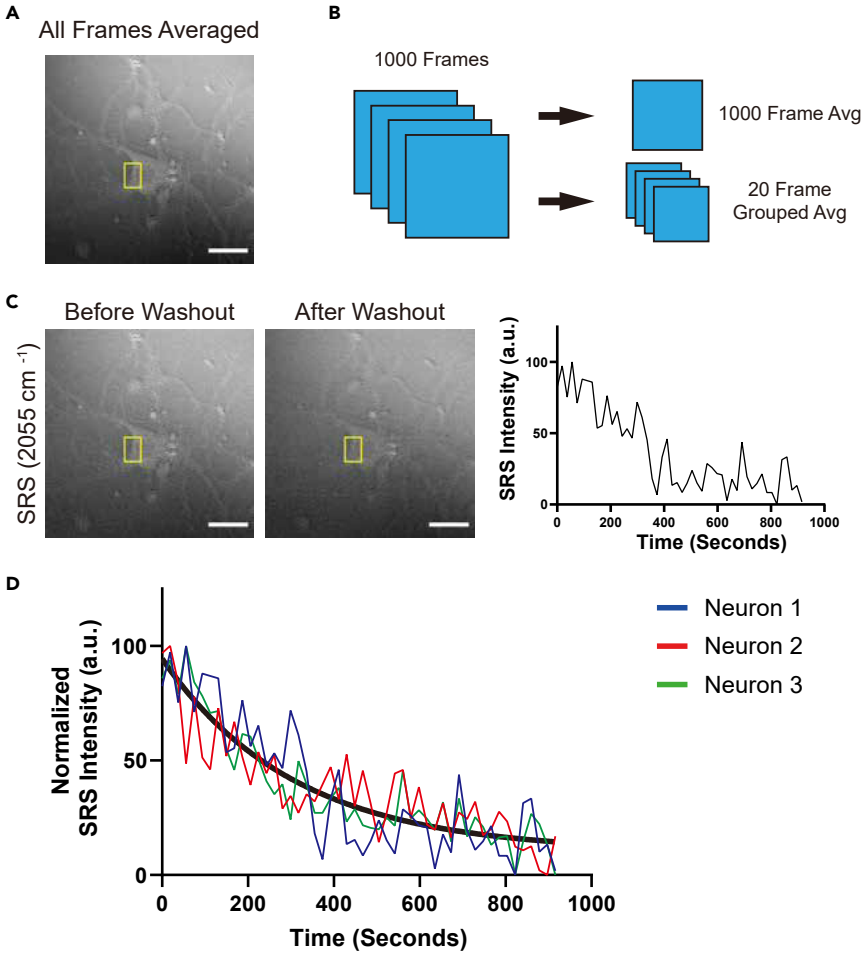

Figure 5. SRS can track dynamics of propofol-d17 binding on live cells

(A) Neurons were imaged in 100 μM propofol-d17 over 1000 frames while perfused with fresh HEPES ACSF solution with 100 μM of non-deuterated propofol. Images show a single image of all 1000 frames averaged together as well as the first and last grouped average of 20 frames (scale bar = 20μm).

(B) Summary of how images were prepared for analysis. Image created from averaging 600 frames together was used as a guide to create regions of interest (ROI) for propofol concentration analysis.

(C) Average intensity was calculated from ROIs created from grouped average images. Every 20 frames were averaged together and propofol concentrations were obtained from the same ROI by calculating the average intensity. Propofol concentration across the cell body decreased as more propofol was perfused into the imaging chamber (scale bar = 20μm).

(D) Washout experiments were repeated and showed the same decrease in SRS signal from deuterated propofol as fresh non-deuterated propofol was perfused into the chamber. This decrease can be modeled with a first-order exponential decay curve (R^2 = 0.796)

results suggest that after constant perfusion of fresh propofol, the signal of propofol-d17 decreases and will level off at background levels.

Additionally, to further evaluate the kinetics of anesthetic binding based on information obtained from SRS images, washout experiments were performed using the same washout rate with Alexa 594 dye in HEPES ACSF. Images were taken in the same time frame as SRS imaging and the signal of Alexa 594 was graphed. The rate of decay of Alexa 594 represents the rate of liquid that flows in and out of the imaging chamber. When graphed together, the rate of decrease in SRS images is much slower than the rate of the washout of Alexa (Figure S5). These observations reveal the dynamic nature of propofol in living neurons and provide a proof of principle that combination of SRS imaging with Raman probes can be utilized to characterize pharmacokinetics of small-sized drugs at cellular resolution.

DISCUSSION

Even though propofol is routinely used, the precise mechanism of action is still not clearly understood. Fully understanding propofol's mechanism is of high importance because risks still exist that relate to the use of propofol (Perrier et al., 2000; Vernooy et al., 2006). SRS microscopy was utilized to uncover new insights into the mechanism of propofol on neurons. Here, we report the first direct evidence showing propofol and its distribution on living neurons. We also report that the major factor determining the localization of propofol is its affinity to the cell membrane. Finally, by taking advantage of our imaging platform capable of simultaneously imaging both Raman scattering and two-photon absorption of fluorescence, we characterized the dynamics of propofol-d17 in living cells in real time. Our results show that propofol is distributed in a uniform manner along the cell membrane of the entire neuron (Figures 3 and 4). Because propofol is highly lipophilic (Sahinovic et al., 2018), it is possible that propofol could in fact concentrate in the cellular membrane of neurons. This data confirm other reports in the literature that suggest propofol interacts with the plasma membrane (Pavel et al., 2020; Pérez-Isidoro et al., 2014; Tsuchiya and Mizogami, 2013). It should be noted that this data doesn't rule out any specific binding that may occur in the membrane to specific receptors; instead, we believe that this data support a more global theory of anesthetic binding. While specific proteins may be targeted by propofol, it can also interact with the membrane and induce changes through those interactions.

An additional aspect to note about the SRS images is that the concentration estimation was conducted on raw pixel intensities without background correction because determination of the true background signal intensity in individual images is a technical challenge. Currently, we have estimated that the local concentration of propofol-d17 at the cell membrane is about 1.3 times that of the concentration of propofol-d17 in solution. However, this estimation comes from the assumption that the background signal is at zero. The background signal is higher than zero which further increases the ratio of signal of propofol-d17 at the cell membrane to that in solution; our estimation of how concentrated propofol-d17 at the cell membrane is an underestimation and the true localized concentration could be more than 2–3 times as concentrated. While our data represent underestimation, our data still show that propofol does indeed concentrate higher at the cell membrane.

The multi-modal imaging ability of our system further helps verifying this claim by enabling us to simultaneously measure the intensity of two-photon excited fluorescence signals of calcein-AM from the same neurons we imaged with SRS. Because calcein-AM is only fluorescent inside of the cell, the projection of the signal from calcein-AM indicates the boundary of the cell body or neurite. At the border of the cell as indicated by calcein-AM staining, the spike in SRS intensity of propofol-d17 is also observed at the same location (Figure 4). This type of verification is only possible with the use of multi-modal imaging, especially in live samples. This powerful feature of multi-modal multiphoton imaging with SRS imaging capacity can facilitate the characterization of complex biological phenomena by enabling simultaneous multifaceted analyses.

The highly sensitive imaging capacity of our system allowed us to probe the spatiotemporal dynamics of propofol. Because both the onset and offset of propofol-induced sedation is quick (Kanto and Gepts, 1989; Sahinovic et al., 2018), we used a perfusion system to introduce and wash out propofol-d17 on the neuronal culture. Calcium imaging revealed that after induction of propofol, it is possible to reverse the effects of propofol by washing out with fresh HEPES ACSF media (Figure S6). Additionally, propofol has a fast redistribution time and quick metabolism cycle which means that continuous propofol infusion is necessary to maintain sedation (Avramov and White, 1997; Candelaria and Smith, 1995; Lundström et al., 2010). The results from the washout of propofol-d17 (Figure 5) are consistent with these observations and provide experimental support to the pharmacological properties of propofol. To verify that the washout time of propofol was a cell-mediated phenomenon, comparison with washout of Alexa dye was used as a stand-in for the mechanical washout rate of the new HEPES ACSF. The rate of decay for Alexa 594 dye and SRS signals from propofol-d17 are different; this suggests that the rate of washout of propofol is not a reflection of the mechanical washout rate but rather a cell-mediated phenomenon at the cell membrane. We expect that these types of analyses will become valuable tools to characterize molecular understandings of anesthetics and other drugs in the future.

In conclusion, we demonstrate that our imaging platform allows us to image and probe the interactions of propofol with living cells that were previously invisible to traditional techniques. We believe that direct

visualization of propofol is an important addition to our expanding knowledge of anesthetic distribution in neurons and can serve as an important steppingstone in the design of future experiments. The unique and powerful features of SRS-capable multi-modal multiphoton imaging described here are expected to shed new light on the pharmacological understandings of currently used drugs and help to design safer and more potent drugs in the future.

Limitations of our study

As mentioned earlier, the issue of background correction causes our estimation of the concentration of propofol-d17 at the plasma membrane may be lower than expected. Rather than using the assumption that the background signal intensity is zero, determination of the true background signal for individual images would enable a more precise calculation of the concentration of propofol on the membrane.

STAR★METHODS

Detailed methods are provided in the online version of this paper and include the following:

- KEY RESOURCES TABLE
- RESOURCE AVAILABILITY
  - Lead Contact
  - Materials availability
  - Data and code availability
- EXPERIMENTAL MODEL AND SUBJECT DETAILS
  - HeLa cell culture
  - Rat hippocampal neuron cell culture
- METHOD DETAILS
  - Calcium imaging and propofol intervention
  - Immunofluorescence staining of $GABA_A$ receptor
  - Stimulated Raman scattering imaging system
  - SRS measurement of Propofol-d17 spectra
  - Multi-modal SRS imaging of Propofol-d17
  - Multi-modal SRS imaging of palmitic Acid-d31 and Glucose-d6
- QUANTIFICATION AND STATISTICAL ANALYSIS

SUPPLEMENTAL INFORMATION

Supplemental information can be found online at https://doi.org/10.1016/j.isci.2022.103936.

ACKNOWLEDGMENTS

We would like to thank Dr. Yoichiro Abe for providing HeLa cells and Olympus Corporation for technical assistance. Funding was provided by Japan Science and Technology Agency Precursory Research for Embryonic Science and Technology (JST PRESTO) (JPMJPR17G6), Japan Science and Technology Agency Core Research for Evolutional Science and Technology (JST CREST) (JPMJCR1872), and Japan Society for the Promotion of Science Grant-in-Aid for Scientific Research (JSPS KAKENHI) (20K20593, 20H02881).

AUTHOR CONTRIBUTIONS

R.O. & M.N. conceived of the project and wrote the manuscript. M.N. supervised the project and assisted with interpretation of the data. R.O. and W.Z. performed cell culture, imaging of neurons, and data analysis. M.Y. contributed to the supervision and writing of the manuscript. J.S. & Y.O. obtained the Raman spectra of propofol-d17 and contributed to the writing of the manuscript.

DECLARATION OF INTERESTS

The authors have no competing interests to disclose.

Received: September 24, 2021
Revised: January 28, 2022
Accepted: February 14, 2022
Published: March 18, 2022

REFERENCES

Avramov, M.N., and White, P.F. (1997). Use of alfentanil and propofol for outpatient monitored anesthesia care: determining the optimal dosing regimen. Anesth. Analg *85*, 566–572.

Candelaria, L.M., and Smith, R.K. (1995). Propofol infusion technique for outpatient general anesthesia. J. Oral Maxillofac. Surg. *53*, 124–128, discussion 129-130.

Cheng, J.-X., and Xie, X.S. (2015). Vibrational spectroscopic imaging of living systems: an emerging platform for biology and medicine. Science *350*, aaa8870.

Feng, A.Y., Kaye, A.D., Kaye, R.J., Belani, K., and Urman, R.D. (2017). Novel propofol derivatives and implications for anesthesia practice. J. Anaesthesiol Clin. Pharmacol. *33*, 9–15.

Fu, D., Zhou, J., Zhu, W.S., Manley, P.W., Wang, Y.K., Hood, T., Wylie, A., and Xie, X.S. (2014). Imaging the intracellular distribution of tyrosine kinase inhibitors in living cells with quantitative hyperspectral stimulated Raman scattering. Nat. Chem. *6*, 614–622.

Hales, T.G., and Lambert, J.J. (1991). The actions of propofol on inhibitory amino acid receptors of bovine adrenomedullary chromaffin cells and rodent central neurones. Br. J. Pharmacol. *104*, 619–628.

Helfenbein, J., Lartigue, C., Noirault, E., Azim, E., Legailliard, J., Galmier, M.J., and Madelmont, J.C. (2002). Isotopic effect study of propofol deuteration on the metabolism, activity, and toxicity of the anesthetic. J. Med. Chem. *45*, 5806–5808.

Hemmings, H.C., Akabas, M.H., Goldstein, P.A., Trudell, J.R., Orser, B.A., and Harrison, N.L. (2005). Emerging molecular mechanisms of general anesthetic action. Trends Pharmacol. Sci. *26*, 503–510.

Hese, L.V., Theys, T., Absalom, A.R., Rex, S., and Cuypers, E. (2020). Comparison of predicted and real propofol and remifentanil concentrations in plasma and brain tissue during target-controlled infusion: a prospective observational study. Anaesthesia *75*, 1626–1634.

Hill, A.H., and Fu, D. (2019). Cellular imaging using stimulated Raman scattering microscopy. Anal Chem. *91*, 9333–9342.

Hu, F., Wei, L., Zheng, C., Shen, Y., and Min, W. (2014). Live-cell vibrational imaging of choline metabolites by stimulated Raman scattering coupled with isotope-based metabolic labeling. Analyst *139*, 2312–2317.

Hu, F., Shi, L., and Min, W. (2019). Biological imaging of chemical bonds by stimulated Raman scattering microscopy. Nat. Methods *16*, 830–842.

Huser, T., and Chan, J. (2015). Raman spectroscopy for physiological investigations of tissues and cells. Adv. Drug Deliv. Rev. *89*, 57–70.

Kahraman, S., Zup, S.L., McCarthy, M.M., and Fiskum, G. (2008). GABAergic mechanism of propofol toxicity in immature neurons. J. Neurosurg. Anesthesiol *20*, 233–240.

Kanto, J., and Gepts, E. (1989). Pharmacokinetic implications for the clinical use of propofol. Clin-Pharmacokinet *17*, 308–326.

Krasowski, M.D., O'Shea, S.M., Rick, C.E., Whiting, P.J., Hadingham, K.L., Czajkowski, C., and Harrison, N.L. (1997). Alpha subunit isoform influences GABA(A) receptor modulation by propofol. Neuropharmacology *36*, 941–949.

Lugli, A.K., Yost, C.S., and Kindler, C.H. (2009). Anaesthetic mechanisms: update on the challenge of unravelling the mystery of anaesthesia. Eur. J. Anaesthesiol *26*, 807–820.

Lundström, S., Twycross, R., Mihalyo, M., and Wilcock, A. (2010). Propofol. J. Pain Symptom Manage. *40*, 466–470.

Mannocchi, G., Napoleoni, F., Napoletano, S., Pantano, F., Santoni, M., Tittarelli, R., and Arbarello, P. (2013). Fatal self administration of tramadol and propofol: a case report. J. Forensic Leg. Med. *20*, 715–719.

Mizuguchi, T., Nuriya, M., Yasui, M., Iino, T., Ozeki, Y., and Saiki, T. (2021). Sensitive detection of alkyne-terminated hydrophobic drug by surface-enhanced stimulated Raman scattering in cetyltrimethylammonium bromide-coated gold nanorod suspensions. Appl. Phys. Express *14*, 032003.

Nwaneshiudu, I.C., Nwaneshiudu, C.A., and Schwartz, D.T. (2014). Separation and enhanced detection of anesthetic compounds using solid phase micro-extraction (SPME)-Raman spectroscopy. Appl. Spectrosc. *68*, 1254–1259.

Ozeki, Y. (2020). Molecular vibrational imaging by stimulated Raman scattering microscopy: principles and applications [Invited]. Chin. Opt. Lett. COL *18*, 121702.

Ozeki, Y., Dake, F., Kajiyama, S., Fukui, K., and Itoh, K. (2009). Analysis and experimental assessment of the sensitivity of stimulated Raman scattering microscopy. Opt. Express, OE *17*, 3651–3658.

Ozeki, Y., Kitagawa, Y., Sumimura, K., Nishizawa, N., Umemura, W., Kajiyama, S., Fukui, K., and Itoh, K. (2010). Stimulated Raman scattering microscope with shot noise limited sensitivity using subharmonically synchronized laser pulses. Opt. Express, OE *18*, 13708–13719.

Ozeki, Y., Umemura, W., Otsuka, Y., Satoh, S., Hashimoto, H., Sumimura, K., Nishizawa, N., Fukui, K., and Itoh, K. (2012). High-speed molecular spectral imaging of tissue with stimulated Raman scattering. Nat. Photon. *6*, 845–851.

Ozeki, Y., Asai, T., Shou, J., and Yoshimi, H. (2019). Multicolor stimulated Raman scattering microscopy with fast wavelength-tunable Yb fiber laser. IEEE J. Selected Top. Quan. Electronics *25*, 1–11.

Paidi, S.K., Siddhanta, S., Strouse, R., McGivney, J.B., Larkin, C., and Barman, I. (2016). Rapid identification of biotherapeutics with label-free Raman spectroscopy. Anal. Chem. *88*, 4361–4368.

Pavel, M.A., Petersen, E.N., Wang, H., Lerner, R.A., and Hansen, S.B. (2020). Studies on the mechanism of general anesthesia. PNAS *117*, 13757–13766.

Pérez-Isidoro, R., Sierra-Valdez, F.J., and Ruiz-Suárez, J.C. (2014). Anesthetic diffusion through lipid membranes depends on the protonation rate. Sci. Rep. *4*, 7534.

Perrier, N.D., Baerga-Varela, Y., and Murray, M.J. (2000). Death related to propofol use in an adult patient. Crit. Care Med. *28*, 3071–3074.

Pologruto, T.A., Sabatini, B.L., and Svoboda, K. (2003). ScanImage: flexible software for operating laser scanning microscopes. Biomed. Eng. Online *2*, 13.

Raman, C.V., and Krishnan, K.S. (1928). A new type of secondary radiation. Nature *121*, 501–502.

Reitz, M., Velizarov, S., Glück, B., Berg, H., and Brambrink, A.M. (1999). Effects of propofol (intravenous propofol emulsion) on cell membranes measured by electrofusion and electroporation. Arzneimittelforschung *49*, 281–285.

Saar, B.G., Freudiger, C.W., Reichman, J., Stanley, C.M., Holtom, G.R., and Xie, X.S. (2010). Video-rate molecular imaging in vivo with stimulated Raman scattering. Science *330*, 1368–1370.

Saar, B.G., Contreras-Rojas, L.R., Xie, X.S., and Guy, R.H. (2011). Imaging drug delivery to skin with stimulated Raman scattering microscopy. Mol. Pharmaceutics *8*, 969–975.

Sahinovic, M.M., Struys, M.M.R.F., and Absalom, A.R. (2018). Clinical pharmacokinetics and pharmacodynamics of propofol. Clin. Pharmacokinet. *57*, 1539–1558.

Schindelin, J., Arganda-Carreras, I., Frise, E., Kaynig, V., Longair, M., Pietzsch, T., Preibisch, S., Rueden, C., Saalfeld, S., Schmid, B., and Tinevez, J.Y. (2012). Fiji: an open-source platform for biological-image analysis. Nature methods *9*, 676–682.

Shou, J., Oda, R., Hu, F., Karasawa, K., Nuriya, M., Yasui, M., Shiramizu, B., Min, W., and Ozeki, Y. (2021). Super-multiplex imaging of cellular dynamics and heterogeneity by integrated stimulated Raman and fluorescence microscopy. Iscience *24*, 102832.

Thomson, A.M., and Jovanovic, J.N. (2010). Mechanisms underlying synapse-specific clustering of GABAA receptors. Eur. J. Neurosci. *31*, 2193–2203.

Tretter, V., Jacob, T.C., Mukherjee, J., Fritschy, J.-M., Pangalos, M.N., and Moss, S.J. (2008). The clustering of GABAA receptor subtypes at inhibitory synapses is facilitated via the direct binding of receptor $\alpha 2$ subunits to gephyrin. J. Neurosci. *28*, 1356–1365.

Tsuchiya, H., and Mizogami, M. (2013). Interaction of local anesthetics with biomembranes consisting of phospholipids and cholesterol: mechanistic and clinical implications for anesthetic and cardiotoxic effects. Anesthesiology Res. Pract. *2013*, e297141.

Urban, B.W., Bleckwenn, M., and Barann, M. (2006). Interactions of anesthetics with their targets: non-specific, specific or both? Pharmacol. Ther. *111*, 729–770.

Vernooy, K., Delhaas, T., Cremer, O.L., Di Diego, J.M., Oliva, A., Timmermans, C., Volders, P.G., Prinzen, F.W., Crijns, H.J.G.M., Antzelevitch, C., et al. (2006). Electrocardiographic changes predicting sudden death in propofol-related infusion syndrome. Heart Rhythm *3*, 131–137.

Wei, L., Yu, Y., Shen, Y., Wang, M.C., and Min, W. (2013). Vibrational imaging of newly synthesized proteins in live cells by stimulated Raman scattering microscopy. Proc. Natl. Acad. Sci. U S A. *110*, 11226–11231.

Wróbel, M.S., Gnyba, M., Urniaż, R., Myllylä, T.S., and Jędrzejewska-Szczerska, M. (2015). Detection of propofol concentrations in blood by Raman spectroscopy. In Clinical and Biomedical Spectroscopy and Imaging IV, J.Q. Brown and V. Deckert, eds. (International Society for Optics and Photonics)), p. 95370Z.

Yang, E., Granata, D., Eckenhoff, R.G., Carnevale, V., and Covarrubias, M. (2018). Propofol inhibits prokaryotic voltage-gated Na+ channels by promoting activation-coupled inactivation. J. Gen. Physiol. *150*, 1299–1316.

Yang, L., Liu, H., Sun, H.-Y., and Li, G.-R. (2015). Intravenous anesthetic propofol inhibits multiple human cardiac potassium channels. Anesthesiology *122*, 571–584.

Yip, G.M.S., Chen, Z.-W., Edge, C.J., Smith, E.H., Dickinson, R., Hohenester, E., Townsend, R.R., Fuchs, K., Sieghart, W., Evers, A.S., et al. (2013). A propofol binding site on mammalian GABA A receptors identified by photolabeling. Nat. Chem. Biol. *9*, 715–720.

Zhang, C., and Cheng, J.-X. (2018). Perspective: coherent Raman scattering microscopy, the future is bright. APL Photon. *3*, 090901.

Zhang, D., Slipchenko, M.N., and Cheng, J.-X. (2011). Highly sensitive vibrational imaging by femtosecond pulse stimulated Raman loss. J. Phys. Chem. Lett. *2*, 1248–1253.

Zhang, F., Wang, C., Cui, Y., Li, S., Yao, Y., Ci, Y., Wang, J., Hou, W., Wu, A., and Li, E. (2016). Effects of propofol on several membrane characteristics of cervical cancer cell lines. CPB *40*, 172–182.

Zhang, L., Shi, L., Shen, Y., Miao, Y., Wei, M., Qian, N., Liu, Y., and Min, W. (2019). Spectral tracing of deuterium for imaging glucose metabolism. Nat. Biomed. Eng. *3*, 402–413.

STAR★METHODS

KEY RESOURCES TABLE

REAGENT or RESOURCE	SOURCE	IDENTIFIER
Antibodies		
Anti-GABA-subunit β3 rabbit antibody	abcam	Cat# Ab104659; RRID:AB_10974605
Anti-rabbit Alexa 488 goat antibody	Thermo Fisher	Cat# A-11008; RRID:AB_143165
Biological samples		
Rat Hippocampal Neurons	Lonza	R-Hi-501
Chemicals, peptides, and recombinant proteins		
Propofol-d17	Toronto Research Chemicals	P829752
Palmitic acid-d31	Toronto Research Chemicals	P144501
Glucose-d6	Cambridge Isotope Laboratories	DLM-2062-1
Fluo-4	Thermo-Fisher	F14201
Alexa-594 Hydrazide	Thermo-Fisher	A10438
Calcein-AM	Thermo-Fisher	C1430
Dimethylsulfoxide	Thermo-Fisher	B10107B
Experimental models: Cell lines		
Human: HeLa cells	RIKEN BRC	0007
Software and algorithms		
Fiji	(Schindelin et al., 2012)	https://imagej.net/Fiji
ScanImage	Pologruto et al., 2003	http://scanimage.vidriotechnologies.com/
Other		
Olympus FV1000	Olympus	1-U2M583

RESOURCE AVAILABILITY

Lead Contact

Further information and requests for resources and reagents should be directed to and will be fulfilled by lead contact, Robert Oda (rwoda@keio.jp)

Materials availability

No new reagents were generated from this paper.

Data and code availability

- All data reported in this paper will be shared by the lead contact upon request.
- This paper does not report original code.
- Any additional information required to reanalyze the data reported in this paper is available from the lead contact upon request.

EXPERIMENTAL MODEL AND SUBJECT DETAILS

HeLa cell culture

HeLa cells (RIKEN BRC Cell Bank, RCB0007) were maintained in 6 cm polystyrene cell culture plates in cell media comprised of DMEM-High Glucose (Thermo Fisher), 10% fetal bovine serum (FBS) (Sigma) and 1% penicillin and streptomycin (P/S) (Nacalai-Tesque). Cells were maintained at 37°C and 5% CO_2. Before imaging, cells were incubated with 1 mL of 0.25% Trypsin/EDTA solution for 1 min at 37°C, collected with 4 mL of cell media and centrifuged at 10,000 RPM for 5 min. Cells were then seeded onto glass bottom

cell culture dishes which were pre coated with 100 μg/mL of poly-L-lysine. Cells were maintained up to a maximum of 13 days and had cell media replaced every 2-3 days.

Rat hippocampal neuron cell culture

Eight 35 mm cell culture dish each containing four collagen-coated coverslips (Iwaki) were initially coated with 30 μg/mL poly-L-lysine filter sterilized in borate buffer in a 35 mm cell culture dish at 37°C. After incubation for an hour, poly-L-lysine/borate buffer was removed from the dishes. 1.5 mL of PNGM media supplemented with NSF-1 (Lonza) was added to the dish to wash out residual poly-L-lysine. Before final plating of hippocampal neurons, this media was removed. A tube of rat hippocampal neurons (Lonza R-Hi-501) were thawed in a 37°C water bath for about 2 min and transferred to a 50 mL conical tube. While stirring the tube gently, 16 mL of NSF-1/PNGM media was slowly added to the cells to prevent osmotic shock. After all the media was added, 2 mL of cells were added to each plate containing coverslips. After incubating in 37°C for about 4 h, 1.5 mL of media was removed from each plate and 2 mL of fresh NSF-1/PNGM media was added. Cells were incubated at 37°C and 5% CO_2 for 10–14 days before imaging. To maintain the cells, 0.75 mL of media was removed and 1 mL of NSF-1/PNGM was added once or twice a week while neurons were growing. Neurons were used after a minimum of 10 days and no longer than 4 weeks of culture.

METHOD DETAILS

Calcium imaging and propofol intervention

In a small tube wrapped in aluminum foil, 15 μL of Fluo4-AM (ThermoFisher) was mixed with 1.5 μL of 20% Pluronic in DMSO (ThermoFisher) for 5 min on a vortex mixer. In a new 35 mm cell culture dish,16.5 μL of Fluo4-AM/Pluronic was added to 1.5 mL of artificial cerebral spinal fluid supplemented with HEPES ((4-(2-hydroxyethyl)-1-piperazineethanesulfonic acid)) (HEPES ACSF) containing 150 mM NaCl, 3 mM KCl, 10 mM dextrose, 1 mM $MgCl_2$, 3 mM $CaCl_2$, and 10 mM HEPES for a final concentration of 10 μM Fluo4-AM. Coverslips containing neurons were then transferred into the cell culture dish containing staining solution and incubated for 15–30 min at 37°C and 5% CO_2. After incubation, coverslips were washed briefly with HEPES ACSF and placed on a glass bottom dish containing 3 mL of HEPES ACSF.

Confocal images were taken using an Olympus FV1000 imaging system equipped with a 10X objective (1-U2M583 UMPlanFl, Olympus). Spontaneous calcium spikes of neurons were obtained by imaging neurons for 600 frames (0.903 frames/second). Images were then analyzed in ImageJ and results were plotted using Prism GraphPad.

To analyze the effects of propofol, 100 mM stock solution of propofol was made in DMSO. Before adding to cells, propofol stock solution was diluted 10 times in HEPES ACSF to make a 10 mM solution of propofol. Cells were first imaged in HEPES ACSF without any drugs. After initial spontaneous calcium signaling in neurons was observed, 30 μL of the 10 mM propofol solution was added to the cell culture dish to make a final concentration of 100 μM of propofol. After propofol was introduced, 600 frames were once again obtained for analysis. To obtain calcium imaging results for propofol-d17 (Toronto Research Chemicals), the same process was performed but with propofol-d17 at the same concentration of 100 μM. For the negative control, DMSO only was added to the culture dishes.

To assess the dynamics of propofol with calcium imaging, neuronal cells were first imaged with HEPES ACSF only for 600 frames. After imaging was completed, fresh HEPES ACSF containing 100 μM propofol was perfused slowly into the cell culture dish using a multi-channel peristaltic pump (Perista) while maintaining 2 mL of solution in the dish. Imaging was done under constant perfusion of propofol for another 600 frames. After imaging, propofol solution was replaced with fresh HEPES ACSF for washout imaging. Imaging was obtained under constant perfusion of fresh HEPES ACSF for a final 600 frames. The same neuronal cell was observed through all three imaging periods.

Immunofluorescence staining of $GABA_A$ receptor

Primary hippocampal neurons and HeLa cells were first washed in HEPES ACSF solution and then fixed in 4% paraformaldehyde in PBS for 15 min at room temperature. After washing in PBS, cells were permeabilized with a cocktail consisting of 10% normal goat serum, 0.5% Triton X-100 and PBS for another 15 min at room temperature. After washing thoroughly with PBS, cells were incubated at room temperature with anti-$GABA_A$ receptor subunit β3 rabbit antibodies (abcam, ab104659) at a concentration of 10μg/mL for

1 h in a cocktail of 2% normal goat serum and 0.1% Triton X-100 in PBS. After incubation of primary antibody, cells were washed three times with PBS for 5 min and then incubated with anti-rabbit immunoglobulin goat antibodies conjugated to Alexa 488 (ThermoFisher) for 1 h at room temperature in the same antibody cocktail solution. After secondary antibody incubation, cells were washed three times with PBS for 5 min and imaged in a glass bottom cell culture dish filled with 2 mL of PBS. Imaging was performed on the confocal imaging system as described above (Olympus FV1000). Fluorescent intensity was calculated by creating a mask using the Otsu method in ImageJ and calculating the average signal intensity. Results were graphed on GraphPad Prism.

Stimulated Raman scattering imaging system

Here we describe our SRS system which is based on previously reported designs (Mizuguchi et al., 2021; Ozeki et al., 2009, 2010). The primary laser in the SRS system is an Emerald ENGINE Ytterbium based laser system (APE) that outputs two laser pulses at 1031 and 516 nm at a repetition rate of 76 MHz. A pump beam is generated by sending the 516 nm pulses through a tunable optical parametric oscillator that can control the wavelength of the output beam for different Raman wavenumbers. The power of pump pulses is controlled by a half waveplate and an analyzer: by adjusting the polarization of the beam with the half waveplate, we can control the power of the pump pulses. The Stokes beam is enlarged using two lenses and controlled using a delay line to synchronize with the pump pulses. Intensity modulation of the Stokes beam is accomplished by passing through an electro-optic modulator (EOM) (Thorlabs, EO-AM-R-38-C2). The EOM is driven by an electrical signal at half the repetition rate (i.e., 38 MHz), which is generated by dividing the frequency of the synchronization signal of the laser. The power of the Stokes beam is also controlled with a half waveplate and analyzer in series. The Stokes and pump pulses are combined spatially with a dichroic mirror and controlled by a galvanometric two-dimensional scanner.

A custom-made Thorlabs microscope system with an automated xyz stage is used as the main microscope platform. The beams are passed through two 25X objectives (XLPLN25XWMP, Olympus) placed below the chamber to illuminate the sample and another objective lens of the same specification was placed above to collect transmitted light and fluorescent signals. The pump laser source had a final power of 150 mW, and the Stokes source had a power of 200 mW after the dichroic mirror before the scanner; the power was reduced by approximately 50% through the scanner and objective lenses. 4 photomultiplier tubes as well as photodiode are arranged in two sets of two on the upper and lower portions of the objective mount. To collect calcein-AM fluorescence signals, a 520–550 nm bandpass filter (BP520-550, ThorLabs) was used on one of the photomultiplier tubes. Intensity of transmitted pump beams is monitored in a photodiode detector (Hamamatsu, S3399) equipped with a custom-made filter/amplifier circuit mounted on the top of the microscope and used to obtain SRS signals using a custom-made lock-in amplifier. The microscope is controlled by the Thorlabs imaging program and ScanImage by Vidrio Technologies for MATLAB (Pologruto et al., 2003). The SRS microscope takes images with dimensions of 512 × 512 pixels at a resolution of 0.617 μm/pixel with a rate of 1.07 frames/second. Lateral resolution of SRS imaging measured using subresolution (~180nm diameter) alkyne beads (Tamagawa Seiki) was 0.55 ± 0.12 μm (mean ± standard deviation). Image processing was completed in Fiji and MATLAB.

SRS measurement of Propofol-d17 spectra

Propofol-d17 was diluted to make a stock solution of 100 mM. On a thin 24 × 60 mm cover glass slide (Matsunami), 5 μL of 100 mM propofol-d17 was pipetted directly on the slide. The propofol-d17 was sandwiched between the glass slide and a 24 × 24 mm cover glass; a 0.1 mm thick imaging spacer (Sigma) separated the two cover glasses. Using a previously described SRS system (Ozeki et al., 2019; Shou et al., 2021), the propofol-d17 spectra was measured between the wavenumbers of 2000–2300 cm^{-1}.

Multi-modal SRS imaging of Propofol-d17

Prior to any treatment with propofol-d17 (Toronto Research Chemicals), cells were subject to loading with fluorescent dyes. Neurons were placed in a 35 mm glass bottom cell culture dish and initially stained with 100 nM calcein-AM (ThermoFisher) in HEPES ACSF for 30 min at room temperature. After incubation, cells were washed in fresh HEPES ACSF and had a final volume of 3 mL of HEPES ACSF added. Immediately prior to imaging, propofol-d17 was added to the cell culture dish to make a final volume of 100 μM propofol-d17. Cells were imaged using SRS and two-photon excited fluorescence. The wavelength of the pump source for the SRS laser was set to 851.2 nm which detects Raman signals at 2055 cm^{-1}. Two-photon fluorescence signals were passed through a band-pass filter and into a PMT. Images were averaged together to create an

image for direct visualization of propofol-d17. Z-stack images were also possible due to an automated xyz-stage; each slice of the z-stack can also be averaged together. Individual images can also be taken and averaged post hoc using imaging software to create time-lapse images. For off-Raman signals the pump laser source was tuned to 855.1 nm which detects Raman signals at 2000 cm^{-1}. Background signals detected at 2000 cm^{-1} were subtracted from signals collected at 2055 cm^{-1}.

For the washout experiment, cells were prepared the same as above and initially imaged with the SRS system for 1000 frames (1.07 frames/second) in HEPES ACSF solution with 100 μM of propofol-d17. Next, using a multi-channel peristaltic pump (Perista), another set of 1000 frames were collected immediately after profusion of fresh HEPES ACSF with 100 μM of regular propofol was started. The same neuronal cell was imaged during the washout of propofol-d17 with regular propofol. To assess the washout speed of the perfusion system, neurons were imaged using the SRS system with an initial solution of 1 μM Alexa 594 in HEPES ACSF. Fresh HEPES ACSF was perfused in, and the neurons were imaged over 1000 frames like above. Each image was averaged together in ImageJ to create a composite image. Grouped averages of 20 frames were created to produce a time-lapse image for analysis. Regions of interest were created using the averaged image as a guide and SRS intensity was measured on the grouped average images using those regions of interest. The calculated and measured intensity of the signal from the ROI created from the grouped averages were collected for each individual cell. Results were graphed using Prism GraphPad with the highest intensity of signal set to a value of 100 and the lowest intensity signal set to a value of 0. The modelling of the exponential decay-curve and R^2 value was also conducted in GraphPad using built-in functions.

Multi-modal SRS imaging of palmitic Acid-d31 and Glucose-d6

For palmitic acid-d31 (Toronto Research Chemicals) imaging, HeLa cells that were plated on glass bottom cell culture dishes were incubated overnight with 100 μM of palmitic acid-d31. After overnight incubation, HeLa cells were then washed with HEPES ACSF and incubated with 100 nM calcein-AM for 30 min at 37°C. After incubation with calcein, cells were washed with HEPES ACSF and imaged in 3 mL of HEPES ACSF using our multi-modal SRS system. SRS imaging was conducted at on-Raman peak of 2,100 cm^{-1} and an off-Raman peak of 2,000 cm^{-1}. A total of 100 images were averaged together to create the final image (1.07 frames/second).

For glucose-d6 (Nacalai-Tesque) imaging, HeLa cells were first washed with Tris-Buffered Saline (TBS) and incubated in TBS for 1 h at 37°C for glucose starvation. After initial glucose starvation, cells were washed in TBS and incubated with 1 mM of glucose-d6 in TBS for another hour at 37°C. During the final 30 min of glucose incubation, calcein-AM was added to the culture dish and incubated for the remaining 30 min. After incubation with both glucose and calcein-AM, cells were washed one final time with HEPES ACSF and immediately imaged using our multi-modal SRS system in 3mL of HEPES ACSF. SRS imaging was conducted at on-Raman peak of 2,150 cm^{-1} and an off-Raman peak of 2,000 cm^{-1}. A total of 100 images were averaged together to create the final image (1.07 frames/second).

QUANTIFICATION AND STATISTICAL ANALYSIS

For image analysis, all images were processed in ImageJ using built-in functions with the program. Details of the process for obtaining concentration of propofol and statistical tests are described in the main text, the STAR Methods sections, and the figure legends.